Annals of Biomedical Engineering, Vol. 28, pp. 495–511, 2000
Printed in the USA.

0090-6964/2000/28(5)/495/17/$15.00

Staged Growth of Optimized Arterial Model Trees

RUDOLF KARCH,[1] FRIEDERIKE NEUMANN,[1] MARTIN NEUMANN,[2] and WOLFGANG SCHREINER[1]

[1]Department of Medical Computer Sciences, University of Vienna, Spitalgasse 23, A-1090 Wien, Austria, and [2]Institute of Experimental Physics, Section for Computational Physics, University of Vienna, Strudlhofgasse 4, A-1090 Wien, Austria

(Received 19 January 1999; accepted 7 April 2000)

Abstract—There is a marked difference in the structure of the arterial tree between epi- and endocardial layers of the human heart. To model these structural variations, we developed an extension to the computational method of constrained constructive optimization (CCO). Within the framework of CCO, a model tree is represented as a dichotomously branching network of straight cylindrical tubes, with flow conditions governed by Poiseuille's law. The tree is grown by successively adding new terminal segments from randomly selected points within the perfusion volume while optimizing the geometric location and topological site of each new connection with respect to minimum intravascular volume. The proposed method of ''staged growth'' guides the generation of new terminal sites by means of an additional time-dependent boundary condition, thereby inducing a sequence of domains of vascular growth within the given perfusion volume. Model trees generated in this way are very similar to reality in their visual appearance and predict diameter ratios of parent and daughter segments, the distribution of symmetry, the transmural distribution of flow, the volume of large arteries, as well as the ratio of small arterial volume in subendocardial and subepicardial layers in good agreement with experimental data. From this study we conclude that the method of CCO combined with staged growth reproduces many characteristics of the different arterial branching patterns in the subendocardium and the subepicardium, which could not be obtained by applying the principle of minimum volume alone. © *2000 Biomedical Engineering Society.* [S0090-6964(00)00805-5]

Keywords—Heart, Epicardial and endocardial differences, Vascular growth model, Mathematical model, Computer simulation, Constrained constructive optimization.

INTRODUCTION

Arterial trees—like other organs—are a result of millions of years of evolutionary design and optimization.[30] As such, they represent highly complex branching structures that fulfill their task of carrying blood to the tissue and removing metabolic end products in a very efficient way.[20,45]

Differences in the branching pattern of vascular trees not only reflect specific metabolic needs of various organs, but also indicate intraorgan variations regarding the demands of perfusion, e.g., epi- and endocardial layers of the vasculature in the human heart exhibit a pronounced difference in structure, adapted to the requirements of blood supply to the beating heart.[6,55] Realistic models of arterial trees therefore call for an adequate representation of such structural features.

Previous models of the coronary arterial tree were based on fractal approaches[44] and on computer-generated trees constructed from experimentally determined morphological properties.[18,43] These models successfully reproduced flow heterogeneity as well as important structural and functional parameters of the coronary tree, but no attempt was made to model its spatial organization, in particular the differences between subendocardial and subepicardial tree structures.

The approach taken by the method of constrained constructive optimization (CCO) (Ref. 31) to model arterial trees draws on optimization principles, which have long been hypothesized for single bifurcations in arterial trees.[24,48] Using the computational method of CCO, we were able to generate—without the direct input of anatomical data—arterial model trees of uniform structure, which were shown to predict important properties of real arterial trees, such as segment radii[15,32] and branching angle statistics.[33] Within the framework of CCO, a model tree is constructed by adding a sequence of individual segments in a stepwise fashion at randomly selected sites within a given perfusion volume. At each step, optimization principles along with a set of constraints and boundary conditions for pressures and flows are applied, which finally determine the geometry and the topological site of each new permanent connection.

A possible way to account for structural variations in the computer model is to interpret vascular growth as being induced by the perfusion demand of the local environment, i.e., by the mutual interaction of structure and hemodynamics, and to couple the CCO algorithm to hemodynamic simulations at each step of tree generation. However, in the light of today's computer facilities, this approach is far from being manageable, especially for high-resolution CCO trees. In the present study we there-

Address correspondence to Rudolf Karch, Department of Medical Computer Sciences, University of Vienna, Spitalgasse 23, A-1090 Wien, Austria. Electronic mail: rudolf.karch@akh-wien.ac.at

fore propose an alternate and more heuristic way to model such structural variations: rather than directly accounting for the impact of the myocardial contraction on the morphology of our model trees, we restrict the generation of new terminal sites to a prescribed sequence of (growing) subsets of the respective perfusion volume (''domains'' of vascular growth) with the aid of an additional (time-dependent) boundary condition, implemented by an appropriate stochastic process.[28] In a previous study,[36] the method of CCO has been applied to model the anatomical variability encountered in real arterial trees by means of different pseudorandom number sequences with identical probability distributions. This work has shown that the structure of CCO-generated trees not only depends on the underlying distribution, but sensitively responds to the actual sequence of new terminal sites. Hence, one might expect that an appropriate time-varying boundary condition for the generation of new terminals would cause a certain variation in the overall tree structure.

In the following, we first briefly review the algorithm used for model tree generation. Then we demonstrate how a modification in the underlying probability distribution for terminal sites from a stationary to a nonstationary form—under otherwise unchanged conditions—leads to certain structural variations both within two- and three-dimensional model trees. Taking advantage of the fact that CCO trees provide segment coordinates and radii in full detail, we finally present a more quantitative analysis of the structures generated with the modified algorithm and compare them with experimental data of the coronary arterial tree.

METHODS

Constrained Constructive Optimization

The method of CCO represents arterial trees as binary branching trees of nonintersecting, rigid cylindrical tubes (''segments'') and does not consider the precise geometric form of individual segments and bifurcations. Likewise, the details of blood rheology and hemodynamics are neglected and blood is modeled as an incompressible, homogeneous Newtonian fluid at steady-state and laminar flow conditions, with Poiseuille's law employed to calculate the hydrodynamic resistance of individual segments.

Although no direct information from topographic anatomy enters the model, CCO maintains a set of boundary conditions and constraints during each step of tree generation: (a) N_{term} perfusion sites are randomly distributed within the given perfusion volume and supplied by N_{term} terminal segments (yielding $N_{\text{tot}}=2N_{\text{term}}-1$ segments in total). (b) Each terminal segment i drains an individual amount of blood flow $Q_{\text{term},i}$ into the microcirculation at the same pressure p_{term}. (c) The total hydrodynamic resistance of the tree is calculated so that either a prescribed pressure difference $\Delta p=p_{\text{perf}}-p_{\text{term}}$ between the inlet and the terminals or a prescribed radius r_{root} of the inlet segment produces a given total perfusion flow Q_{perf}. (d) At each bifurcation, the radii of parent and daughter segments obey a power law of the form[25,38]

$$r_{\text{parent}}^{\gamma}=r_L^{\gamma}+r_S^{\gamma}, \tag{1}$$

with a constant exponent $\gamma>0$ (bifurcation exponent), where r_L and r_S are the radii of the ''larger'' and ''smaller'' daughter segments, respectively (i.e., $r_L \geqslant r_S$).

Growing a model tree by CCO basically consists of a finite sequence of two tightly coupled steps: (i) growth and (ii) constrained optimization. To generate the very first segment of the tree, a randomly selected point from the interior of the perfusion volume V is connected to a fixed point at the boundary of V. This point represents the inlet to the tree, i.e., the proximal end of the tree's root segment. Growth is continued by successively adding new terminal segments, each of which connects a randomly chosen point within V to one of the existing segments, thus creating a new bifurcation somewhere along that segment. Both the segment to which a new connection is established and the final position of the bifurcation are found by optimizing a prescribed target function T, calculated from the tree generated so far. In the present study, we consider the total intravascular volume as the optimization target to be minimized,[14]

$$T=\pi\sum_{i=1}^{N_{\text{tot}}} l_i r_i^2, \tag{2}$$

where l_i and r_i denote length and luminal radius of segment i. A detailed description of the algorithm of CCO has been given elsewhere.[15,32]

The Concept of Staged Growth

The original method of CCO generates arterial model trees of homogeneous structure, where segments from the very early stages of construction turn into the main vessels of the final trees. This observation suggests a possible (though heuristic) approach for the simulation of structural variations: rather than sampling new terminal locations $\mathbf{x}$ from a given (e.g., uniform) spatial distribution with probability density function (PDF) $f(\mathbf{x})$ over the whole perfusion volume V, we restrict the generation of new terminal sites to a prescribed sequence of subsets $V_\lambda \subseteq V$ (''domains of vascular growth,'' Fig. 1). The specific shape and sequence of these growth domains then determines the resulting structural properties of the model trees (e.g., an arrangement of the large arteries at

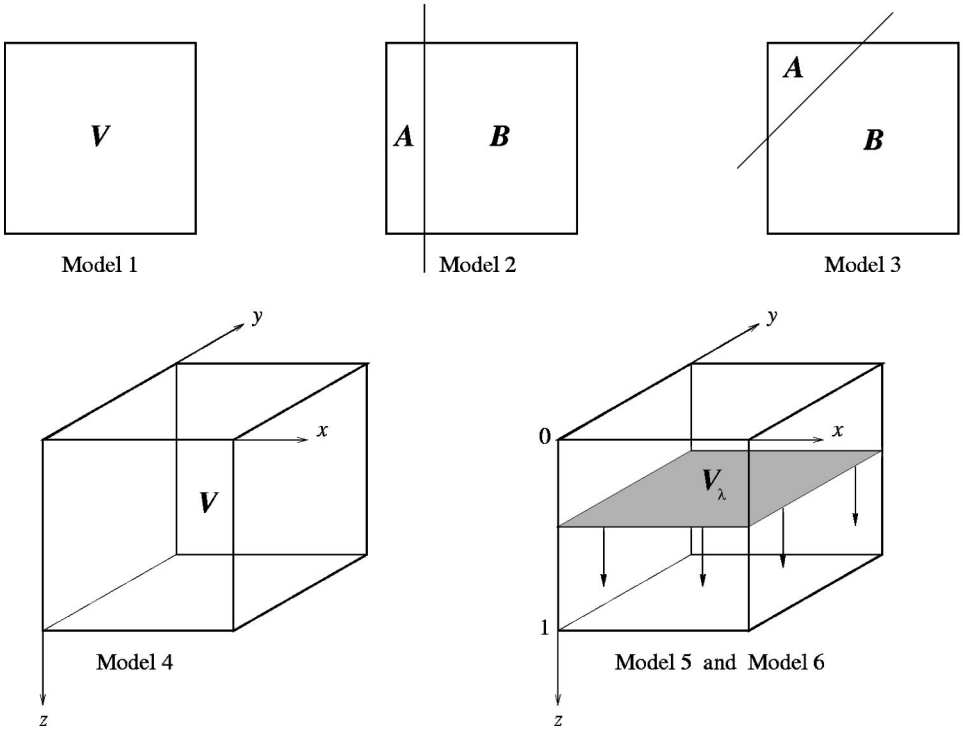

FIGURE 1. Geometries for conventional and staged growth. Top: conventional (left) and staged growth (center, right) in a two-dimensional area *V*; subsets *A* and *B* of *V* represent two disjoint domains of vascular growth. Bottom: conventional (left) and staged growth (right) in a three-dimensional model for the arterial tree in a piece of tissue of the myocardial wall; a thin layer of growth V_λ parallel to the epicardial surface ($z=0$) is gradually enlarged towards the endocardial surface ($z=1$).

the surface of the perfusion volume can be achieved by defining a surface layer as the primary growth domain). To implement this concept of ''staged growth,'' we consider an appropriate stochastic process for the generation of new terminal sites, characterized by a time-dependent PDF $g(\mathbf{x},\lambda(t))$, which (i) induces a proper sequence of growth domains and (ii) still maintains the prescribed spatial distribution $f(\mathbf{x})$ of terminals. Note that we cannot simply use the given probability distribution $f(\mathbf{x})$ within each domain, since the varying size of successive domains would cause the final spatial distribution of terminals to be considerably biased relative to $f(\mathbf{x})$.

The Algorithm of Staged Growth

Let $f(\mathbf{x})$ denote a prescribed PDF that the final distribution of terminal locations $\mathbf{x}$ should follow within the given perfusion volume V. [Note that the actual distribution of terminal sites at any stage of tree generation will be biased to a certain extent with respect to $f(\mathbf{x})$ due to the history of the process, i.e., the preexisting tree structure that new terminal sites must not coincide with.] Rather than directly sampling new terminal locations from $f(\mathbf{x})$, we use a family $g(\mathbf{x},\lambda)$ of PDFs, defined on certain subsets $V_\lambda \subseteq V$ with $\cup_\lambda V_\lambda = V$, i.e., we interpret the random variable $\mathbf{x}$ as the outcome of a combined stochastic process: first, a value for λ is chosen and then $\mathbf{x}$ is sampled from $g(\mathbf{x},\lambda)$. Thus $g(\mathbf{x},\lambda)$ is the conditional PDF of $\mathbf{x}$ given λ. Specifically, we consider a family $\mathbf{x}_\lambda$ of random variables with PDF $g(\mathbf{x},\lambda)$ and with values in V,

$$g(\mathbf{x},\lambda) \geqslant 0, \tag{3}$$

$$\int_V g(\mathbf{x},\lambda)\, d\mathbf{x} = 1, \tag{4}$$

where the parameter λ, $0 \leqslant \lambda \leqslant 1$, represents another random variable with PDF $p(\lambda)$,

$$p(\lambda) \geqslant 0, \tag{5}$$

$$\int_0^1 p(\lambda)\, d\lambda = 1. \tag{6}$$

Then the overall PDF $f(\mathbf{x})$ for the result of our combined process is given by

$$f(\mathbf{x}) = \int_0^1 p(\lambda) g(\mathbf{x},\lambda) d\lambda \geqslant 0. \tag{7}$$

From Eqs. (4) and (6) it follows that

$$\int_V f(\mathbf{x}) d\mathbf{x} = \int_V \int_0^1 p(\lambda) g(\mathbf{x},\lambda) d\lambda d\mathbf{x} = \int_0^1 p(\lambda) d\lambda = 1, \tag{8}$$

hence $f(\mathbf{x})$ is properly normalized.

In general, there are various ways for defining $g(\mathbf{x},\lambda)$ and $p(\lambda)$ to generate a prescribed objective distribution $f(\mathbf{x})$ compatible with Eqs. (7) and (8). Since the sequence of domains of vascular growth as well as the resulting vascular structures depend on the specific realization of the sample from $p(\lambda)$, we vary the parameter λ on a systematic rather than on a random basis. For this reason, we introduce a function

$$\lambda : [0,T] \to [0,1], t \mapsto \lambda(t), \tag{9}$$

which will be called ''protocol.'' $t \in [0,T]$ indicates the current ''time'' or—equivalently—the number of terminal segments generated thus far during the course of tree development and T corresponds to the final total number of terminals N_{term}. Since the relative frequency of λ is inversely proportional to the rate of change $d\lambda/dt$ of $\lambda(t)$, the respective PDF $p(\lambda)$ is given by

$$p(\lambda) = \frac{1}{T}\left(\frac{d\lambda}{dt}\right)^{-1}, \tag{10}$$

and the overall PDF for the process $\mathbf{x}=\mathbf{x}(\lambda(t))$ can be written as

$$f(\mathbf{x}) = \int_0^1 p(\lambda) g(\mathbf{x},\lambda) d\lambda = \frac{1}{T}\int_0^T g(\mathbf{x},\lambda(t)) dt. \tag{11}$$

To demonstrate the concept of a time-dependent PDF $g(\mathbf{x},\lambda(t))$ for the simulation of vascular growth within the framework of CCO we first discuss some straightforward and illustrating examples in one and two dimensions and then focus on a more realistic model concerning the arterial structure in the myocardial wall.

Example 1: Uniform Distribution in 1D. To generate a resulting distribution of $f(x) \equiv 1$ for a one-dimensional (1D) uniformly distributed random variable $x \in V = [0,1]$ we may choose for V_λ the set consisting of the single point $x = \lambda$ and move λ with constant velocity from $\lambda = 0$ to $\lambda = 1$. Hence, we obtain the following process $x(\lambda(t))$:

$$g(x,\lambda) = \delta(x-\lambda), \tag{12}$$

$$\lambda(t) = \frac{t}{T}, \tag{13}$$

where $\delta(x-\lambda)$ denotes the Dirac delta function and $0 \leqslant t \leqslant T$. Here the subsets $V_\lambda \subseteq V$ degenerate to a sequence of points, and the resulting PDF $f(x)$ is given by

$$f(x) = \frac{1}{T}\int_0^T \delta\left(x - \frac{t}{T}\right) dt = 1. \tag{14}$$

An alternative approach involving a family V_λ of ''monotonically increasing'' nondegenerate subsets which systematically ''fill'' V might be based on intervals of the form $V_\lambda = [0,\lambda]$ such that

$$V_\lambda \subseteq V_{\lambda'} \quad \text{for } \lambda \leqslant \lambda'. \tag{15}$$

For instance, consider the process $x(\lambda(t))$ with a power-law PDF [cf. Fig. 2(a)]

$$g(x,\lambda) = \frac{(\alpha+1)x^\alpha}{\lambda^{\alpha+1}}\Theta(\lambda - x). \tag{16}$$

Here $\Theta(x)$ denotes the Heaviside unit step function [i.e., $\Theta(x) = 1$ for $x \geqslant 0$ and $\Theta(x) = 0$ for $x < 0$] and $\alpha > 0$ is an additional parameter. In particular, if $p(\lambda) = 1$, the overall PDF $f(x)$ is obtained as [cf. Fig. 2(c)]

$$f(x) = \int_0^1 p(\lambda) g(x,\lambda) d\lambda = \frac{\alpha+1}{\alpha}(1 - x^\alpha). \tag{17}$$

For $p(\lambda) = 1$, however, the overall distribution of x cannot be uniform. Therefore, we restrict ourselves to the most simple case $\alpha = 1$ and construct a special protocol function $\lambda(t)$ so as to render $p(\lambda)$ nonuniform [cf. Figs. 3(a) and 3(b)]:

$$g(x,\lambda) = \frac{2x}{\lambda^2}\Theta(\lambda - x), \tag{18}$$

$$\lambda(t) = \begin{cases} \dfrac{2t}{T} & \text{for } 0 < t \leqslant T/2, \\ 1 & \text{for } T/2 < t \leqslant T. \end{cases} \tag{19}$$

For $0 < \lambda \leqslant 1$ the functions $g(x,\lambda)$ of Eq. (18) represent a sequence of triangles with decreasing height and in-

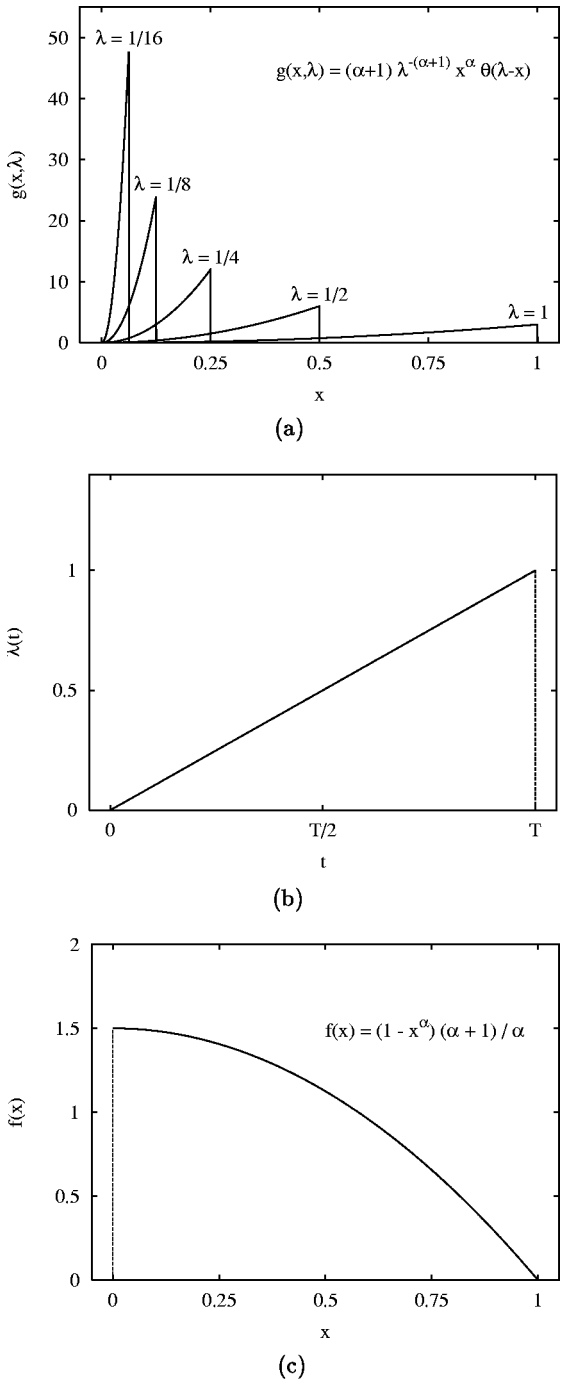

FIGURE 2. (a) **Power-law PDF** $g(x,\lambda)=(\alpha+1)\lambda^{-(\alpha+1)}x^{\alpha}\Theta(\lambda-x)$, **Eq. (16), displayed for** $\alpha=2$ **and for selected values of the parameter** λ. (b) **Protocol function** $\lambda(t)=t/T$, $0\leq t\leq T$, **with** $p(\lambda)=1$. (c) **Resulting overall PDF** $f(x)=(1-x^{\alpha})(\alpha+1)/\alpha$, **Eq. (17), displayed for** $\alpha=2$.

creasing base. From the protocol function $\lambda(t)$, Eq. (19), we obtain the corresponding PDF of λ as

$$p(\lambda)=\tfrac{1}{2}[1+\delta(\lambda-1)]. \tag{20}$$

Now the resulting PDF $f(x)$ is uniform, since

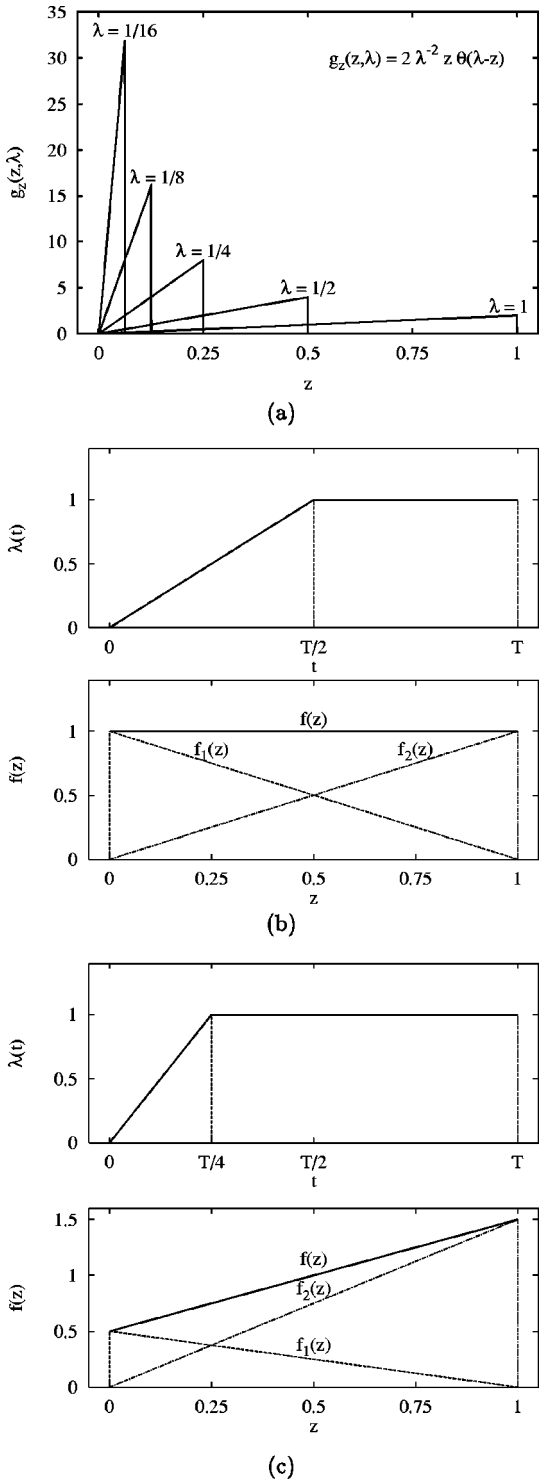

FIGURE 3. (a) **The PDF for tossing normalized** z **coordinates,** $g_z(z,\lambda)=2\lambda^{-2}z\Theta(\lambda-z)$, **Eq. (30), is displayed for selected values of the parameter** λ. (b) **Protocol function** $\lambda(t)$, **Eq. (19), and resulting overall PDF** $f(z)=1$, **obtained as the sum of** $f_1(z)=(1-z)$ **and** $f_2(z)=z$, **where** $f_1(z)$ **and** $f_2(z)$ **denote the overall PDF for the interval** $0<t\leq T/2$ **and** $T/2<t\leq T$, **respectively [cf. Eq. (21)].** (c) **Protocol function** $\lambda(t)$, **Eq. (22), and corresponding overall PDF** $f(z)=f_1(z)+f_2(z)=z+1/2$ **with** $f_1(z)=(1-z)/2$ **for** $0<t\leq T/4$ **and** $f_2(z)=3z/2$ **for** $T/4<t\leq T$ **[cf. Eq. (24)].**

$$f(x)=\int_0^1 p(\lambda)\, g(x,\lambda)\,d\lambda=\tfrac{1}{2}\int_0^1 g(x,\lambda)\,d\lambda+\tfrac{1}{2}g(x,1)$$

$$=(1-x)+x=1. \tag{21}$$

Example 2: Linear Distribution in 1D. For a given $g(x,\lambda)$, Eq. (18), the rate at which the protocol function $\lambda(t)$ of Eq. (19) increases from 0 to 1 as well as the proportion of time during which $\lambda(t)=1$ determine the resulting PDF $f(x)$. For instance, a protocol function of the form [cf. Figs. 3(a) and 3(c)]

$$\lambda(t)=\begin{cases}\dfrac{4t}{T} & \text{for } 0<t\leqslant T/4,\\ 1 & \text{for } T/4<t\leqslant T,\end{cases} \tag{22}$$

yields

$$p(\lambda)=\tfrac{1}{4}[1+3\,\delta(\lambda-1)], \tag{23}$$

and therefore results in a linear overall PDF

$$f(x)=\int_0^1 p(\lambda)g(x,\lambda)\,d\lambda=\tfrac{1}{4}\int_0^1 g(x,\lambda)\,d\lambda+\tfrac{3}{4}g(x,1)$$

$$=\tfrac{1}{2}(1-x)+\tfrac{3}{2}x=x+\tfrac{1}{2}. \tag{24}$$

Example 3: CCO Trees Generated by Disjoint Domains of Vascular Growth in 2D. Consider a square perfusion area V in the two-dimensional (2D) plane and let A and B be two subsets of V with $A\cup B=V$ and $A\cap B=\varnothing$ (cf. Fig. 1, upper panels). To generate a uniform overall distribution by means of a growth process that confines terminal sites only in subset A during the initial stage of growth and in subset B during the second (final) stage, we set

$$g(\mathbf{x},\lambda)=\begin{cases}|A|^{-1}I_A(\mathbf{x}) & \text{for } \lambda=0,\\ |B|^{-1}I_B(\mathbf{x}) & \text{for } \lambda=1,\end{cases} \tag{25}$$

$$\lambda(t)=\begin{cases}0 & \text{for } 0<t\leqslant \dfrac{|A|}{|A|+|B|}T,\\ 1 & \text{for } \dfrac{|A|}{|A|+|B|}T<t\leqslant T,\end{cases} \tag{26}$$

where I_A is the indicator function of A, i.e., $I_A(\mathbf{x})=1$ if $\mathbf{x}\in A$ and $I_A(\mathbf{x})=0$ otherwise; $|A|$ and $|B|$ denote the area of A and B, respectively. This special form of $g(\mathbf{x},\lambda)$ splits V into two disjoint domains of vascular growth ($V_1=A$ and $V_2=B$), where A is visited exclusively during the first stage ($\lambda=0$) and B during the second stage ($\lambda=1$) of growth. Although tossing of new terminals is confined to the respective subsets A and B, the connection site of a new terminal segment remains unrestricted; hence, terminal locations originating in B might well be connected to segments in A. Since the time-intervals $\Delta t_1=|A|/(|A|+|B|)T$ for $\lambda=0$ and $\Delta t_2=|B|/(|A|+|B|)T$ for $\lambda=1$ are proportional to the respective areas, $\Delta t_1/\Delta t_2=|A|/|B|$, the terminal locations in the final tree will be homogeneously distributed in V.

Example 4: Application to the Coronary Arterial Tree. It is well known from the anatomy of mammal coronary arteries that large, blood conveying vessels predominantly run at the surface of the myocardium, while numerous smaller branches enter the myocardium almost at right angles to the epicardial surface and usually pass down to the endocardium.[6,12] In addition, the volume of small arteries and arterioles is higher in the subendocardium than in the subepicardium, indicating a better vascularization of the subendocardium.[47] This special anatomical structure allows for an efficient blood supply of the beating heart.

To model this anatomical structure, we consider a piece of tissue between the epi- and endocardial surface of the ventricular wall to be perfused with blood; within our computer model, this piece is represented as a rectangular slab V. We set $g(\mathbf{x},\lambda)$ such as to fill up V by a sequence V_λ of increasing domains of vascular growth, i.e., we choose

$$V_\lambda\subseteq V_{\lambda'} \quad \text{for } \lambda\leqslant\lambda'. \tag{27}$$

Starting from a thin layer parallel to the epicardial surface, $g(\mathbf{x},\lambda)$ should gradually enlarge this initial zone towards the endocardial surface until the whole ventricular wall is incorporated (cf. Fig. 1, lower panels). Due to the specific properties of CCO trees, one would expect this algorithm to arrange the main vessels near the epicardial surface, similar to the morphology of real coronary arteries.

As to the special form of $g(\mathbf{x},\lambda)$, we may assume that

$$g(\mathbf{x},\lambda)=g_x(x)g_y(y)g_z(z,\lambda), \tag{28}$$

since the zones of vascular growth should vary only along the z direction and because all three components of $\mathbf{x}$ should be statistically independent. Moreover, we define normalized coordinates $x,y,z\in[0,1]$ and assume that $z=0$ corresponds to the epicardial surface and $z=1$ to the endocardial surface. (We can therefore think of z as representing the relative wall position within the myocardium.) For the purpose of the present study, we

either assume a uniform resulting distribution of terminals throughout the perfusion volume (i.e., we set $f(z)=1$, ''model 5''), or we prescribe a resulting distribution $f(z)$, which increases linearly from epi- to endocardial layers according to $f(z)=z+1/2$ (''model 6,'' cf. example 2). The latter choice is motivated by the distribution of small arterial volume reported by Wüsten *et al.*[47] (see above) and by transmural flow data reported by Austin *et al.*[2] These authors have shown that in arrested, maximally vasodilated hearts, the endocardial flow is approximately twice that of the epicardial flow. Since our model trees are generated under the assumption of equal terminal flows, the transmural distribution of terminals directly reflects the respective distribution of flow.

New terminal positions $\mathbf{x}=(x,y,z)$ are generated by means of the following algorithm: x and y are sampled from a uniform distribution on $[0,1]$,

$$g_x(x)=g_y(y)=1, \tag{29}$$

and z is determined by the PDF given in Eq. (18),

$$g_z(z,\lambda)=\frac{2z}{\lambda^2}\Theta(\lambda-z), \tag{30}$$

with protocol function $\lambda(t)$ according to Eq. (19) or Eq. (22), cf. Fig. 3.

To sample z with probability density $g_z(z,\lambda)$, Eq. (30), by means of the uniformly distributed random numbers $\xi\in[0,1)$ supplied by the random number generator of the computer, we employ the transformation method $z=z(\xi)$ (e.g., Kalos[13]). Since ξ is uniform, its cumulative distribution function is

$$F(\xi)=\xi, \tag{31}$$

on $[0,1)$, and the functional dependence of z on ξ is determined by solving the equation

$$G(z,\lambda)=F(\xi), \tag{32}$$

for z, where $G(z,\lambda)$ is the cumulative distribution function of z. From Eqs. (16) and (31) we have for $0\leqslant z\leqslant\lambda$

$$G(z,\lambda)=\int_0^z\frac{(\alpha+1)u^\alpha}{\lambda^{\alpha+1}}du=\frac{z^{\alpha+1}}{\lambda^{\alpha+1}}=\xi. \tag{33}$$

This yields the desired transformation $z=G^{-1}(\xi)$:

$$z=\lambda\,\xi^{1/(\alpha+1)}. \tag{34}$$

We finally note that the process $\mathbf{x}(\lambda(t))$ with PDF $g(\mathbf{x},\lambda)$ and protocol function $\lambda(t)$ determines the actual path of growth (i.e., the sequence of domains V_λ) as well as the resulting distribution $f(\mathbf{x})$. For the present study, the special choice of $g(\mathbf{x},\lambda)$, Eqs. (28)–(30), and $\lambda(t)$, Eqs. (19) and (22), generates the coarse ''frame'' of the tree during the first period of growth ($0<t\leqslant T/2$ or $0<t\leqslant T/4$) and fills this initial structure with additional terminals during the second period ($T/2<t\leqslant T$ or $T/4<t\leqslant T$) in such a way that the resulting distribution $f(\mathbf{x})$ is uniform or linearly increasing in the z direction (Fig. 3). Of course, one could as well prescribe different resulting PDFs $f(\mathbf{x})$ and/or $g(\mathbf{x},\lambda)$ and $\lambda(t)$ to generate trees of different structure. However, a systematic study of these variations is beyond the scope of the present paper and is left to future work.

RESULTS

Visual Representation of Structural Changes

As could be demonstrated in previous work, the structure of CCO-generated trees sensitively depends—for a given perfusion volume—on three simulation parameters: (i) the target function, Eq. (2); (ii) the seed of the random number sequence used to generate the distal locations of new terminal segments; and (iii) also on the exponent γ in the bifurcation law, Eq. (1).[27] Interestingly, modifying even a single parameter entails structural changes, sufficiently pronounced to be evident to the naked eye. We therefore begin to describe—on a visual basis—the structural effects of staged growth by means of two- and three-dimensional (3D) model trees which were generated either by ''conventional'' CCO or by staged growth according to the examples given in the previous section (cf. Fig. 1 and Table 1).

Figure 4(a) shows the reference tree for the two-dimensional case (''model 1''), generated by conventional CCO and perfusing a square area V of 10 cm$\times$10 cm in dimension with $N_{\text{term}}=3000$ terminal segments (the simulation parameters are specified in Table 2). The structural variations induced by switching to a nonstationary distribution $g(\mathbf{x},\lambda)$ of the form given in Eqs. (25) and (26) are immediately evident: In Fig. 4(b) $g(\mathbf{x},\lambda)$ splits V into two disjoint vertical rectangular regions A and B with area ratio $|A|/|B|=1/4$ (''model 2,'' see also Fig. 1). While the main vessels of the reference tree branch more or less evenly throughout the perfusion area, the tree in Fig. 4(b) builds up a main vessel near its left boundary during the initial stage of growth when only subset A is accessible for tossing new terminals; during the second stage of growth, additional vessels connect to these existing structures and branch out at almost right angles to perfuse the rest of the model area (corresponding to subset B). The structural changes visible in Fig. 4(c) are even more pronounced (''model 3,''

TABLE 1. Characteristics of model trees.

	Geometry	Dimension (cm)	N_{term}*	Q_{term}† (ml/min)	Growth
Model 1	2D square	10×10	3000	0.167	Conventional
Model 2	2D square	10×10	3000	0.167	Staged
Model 3	2D square	10×10	3000	0.167	Staged
Model 4	3D slab	9×7×1.6	6000	0.083	Conventional
Model 5	3D slab	9×7×1.6	6000	0.083	Staged, uniform PDF
Model 6	3D slab	9×7×1.6	6000	0.083	Staged, linear PDF

*Number of terminal segments in fully developed trees.
†Terminal flow.

see also Fig. 1); here $g(\mathbf{x},\lambda)$ induces a triangular region at the upper left corner of V for the initial subset A and a pentagonal region for the final subset B. This partitioning of V causes the root segment to branch early into two major vessels. During the second stage of growth this structure inherited from the previous stage triggers the development of two large conveying vessels to supply region B.

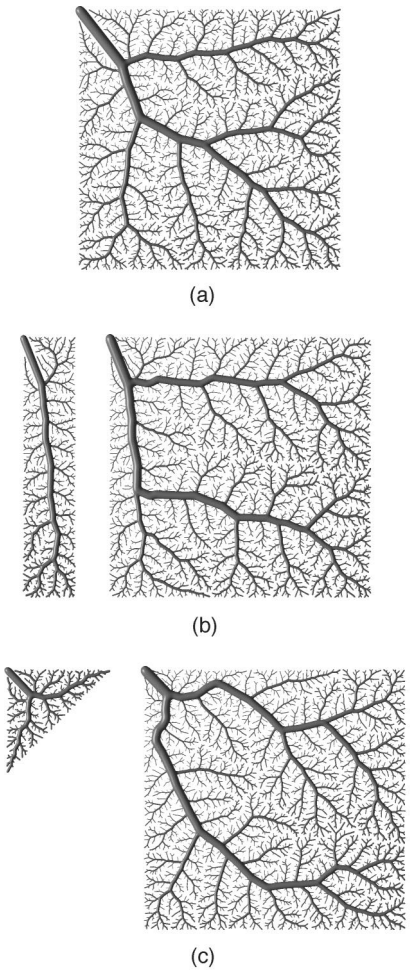

FIGURE 4. Visual representation of two-dimensional staged growth. (a) (Model 1): reference tree grown by conventional CCO. (b) and (c) (models 2 and 3): initial phase of growth in domain *A* (left) and final tree (right). Simulation parameters and geometries are given in Table 1, Table 2, and Fig. 1.

Figure 5 displays a three-dimensional example, designed to represent key structural features of mammal coronary arteries.[26] The reference tree in panel (a) was generated using a uniform and stationary distribution for new terminal sites (''model 4''), whereas for the tree in panel (b) $g(\mathbf{x},\lambda)$ was set according to Eqs. (28)–(30) with protocol function $\lambda(t)$ of Eq. (22), i.e., with a resulting distribution of terminals that linearly increases from epi- to endocardial layers (''model 6,'' see also Fig. 1 and example 2). The perfusion bed was modeled as a rectangular slab of 9 cm×7 cm×1.6 cm, supplied by $N_{term}=6000$ terminal segments under the physiological conditions given in Table 2. N_{term} was chosen on the basis of computational feasibility (computing time for each model was approximately 10 h on a DEC-Alpha 21164/333 MHz CPU) and does not reflect the actual number of end segments, which has been estimated by VanBavel and Spaan[43] to be about three orders of magnitude higher. Therefore, CCO trees will model only the major arteries and a very small portion of the small arteries of coronary arterial trees, and terminal segments of CCO trees have no direct correspondence to end segments of real arterial trees. The total perfusion flow $Q_{perf}=500$ ml/min was set for an arterial tree supplying approximately 100 g of myocardial tissue under cardiac arrest and maximum vasodilation.[5] According to measurements reported for the pig coronary arteries,[16] the radius of the root segment was set to $r_{root}=2$ mm. For the prescribed number of terminals N_{term} and total perfusion flow Q_{perf} this yields the terminal pressures given in Table 3. Blood viscosity was assumed constant over the range of shear rates and vessel radii observed in the model trees.

While the large arteries of the reference tree in the upper panel branch in a more or less unimpeded fashion throughout the perfusion volume, the main vessels in the lower panel, originating from the early stages of tree generation, predominantly run at the ''epicardial'' surface, and give off smaller vessels at almost right angles

TABLE 2. Simulation parameters.

Parameter	Meaning	Value		Source
		Common units	SI units	
p_{perf}	Perfusion pressure	100 mm Hg	1.33×10^{4} Pa	Chilian *et al.* (Ref. 4)
Q_{perf}	Perfusion flow	500 ml/min	8.33×10^{-6} $m^3 s^{-1}$	Chilian (Ref. 5)
r_{root}	Radius of root segment	2 mm	2.00×10^{-3} m	Kassab *et al.* (Ref. 16)
η	Viscosity of blood	3.6 cp	3.60×10^{-3} Pa s	Lipowsky and Zweifach (Ref. 21)
γ	Bifurcation exponent	2.55		Arts *et al.* (Ref. 1)

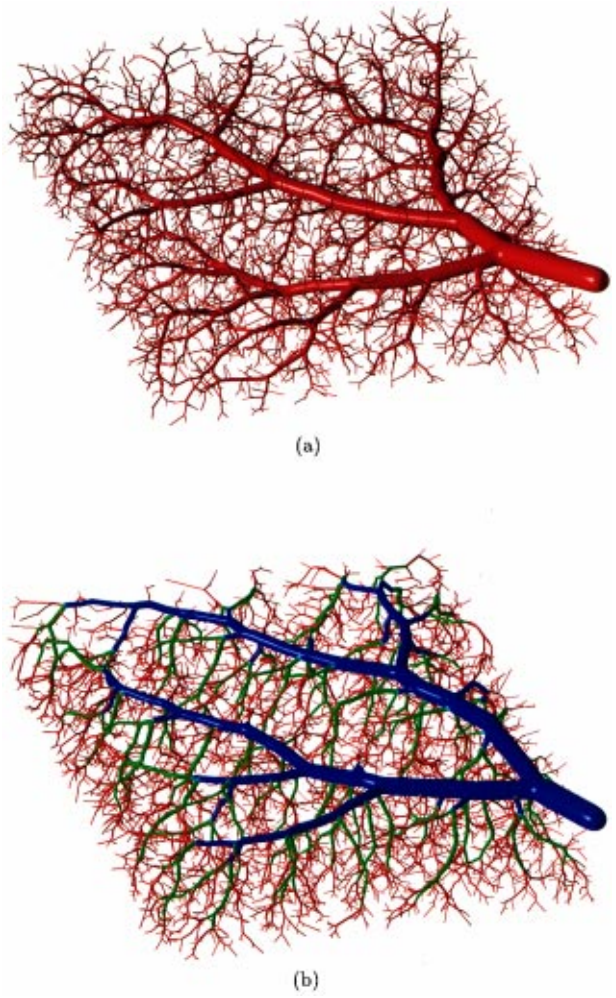

FIGURE 5. Visual representation of three-dimensional staged growth. (a) Reference tree grown by conventional CCO (model 4). (b) Staged growth according to the process $\mathbf{x}(\lambda(t))$ with PDF $g(\mathbf{x},\lambda)$, cf. Eqs. (28)–(30), and protocol function $\lambda(t)$ as given in Eq. (22) (model 6); different colors represent different classes of segments (cf. Fig. 8). Geometries and simulation parameters are given in Table 1, Table 2, and Fig. 1. Visualization was performed by representing the vessel segments as the isosurface of a pseudopotential assigned to the whole tree (see Neumann *et al.*, Ref. 26).

into the interior of the model tissue, similar to the anatomy of real coronary arteries.[6,12,54,55]

So far, visual inspection of the model trees has shown that the structural changes due to a time-dependent probability distribution for the generation of new terminal sites are immediately evident. In the next section we present a more quantitative characterization of these changes as reflected in the variation of certain global morphometric descriptors.

Changes in Global Quantities

The structural differences due to staged growth entail variations of key global quantities, such as total volume, total surface, and sum of segment lengths (Table 3). The structural changes between model 4 and model 5 (model 6) are accompanied by an increase of the total volume and total surface of the trees by 7.3% (8.5%) and 8.5% (7.9%), respectively. The sum of segment lengths slightly increases by about 1.4% (1.3%). The pressure drop between the root segment (i.e., the inlet to the tree) and terminal segments increases by about 1.7% (2.1%), indicating a slightly increased total hydrodynamic resistance of the ''surface-dominated'' structures of models 5 and 6.

The two-dimensional examples for staged growth (models 2 and 3) show similar trends for total volume, total surface, and pressure drop between the root and terminals; the sum of segment lengths remains almost unaffected.

Bifurcation Symmetry

The degree of symmetry of an individual bifurcating segment i is usually expressed by its local symmetry index:[43,52]

$$\xi_{rad}(i)=r_S/r_L, \quad (0<\xi_{rad}\leqslant 1), \tag{35}$$

TABLE 3. Global quantities. The values for models 4, 5, and 6 are mean ±SD for ten realizations of the respective model.

	p_{term}* (mm Hg)	d_{term}† (μm)	Total volume (cm^3)	Total surface (cm^2)	Total length (m)	Max(Λ_{bif})‡
Model 1	92.6	242.30	2.74	105.5	6.81	73
Model 2	92.2	240.54	2.87	106.2	6.81	82
Model 3	92.2	239.48	2.87	106.5	6.84	93
Model 4	79.25±0.06	126.05±0.07	1.65±0.01	101.6±0.2	12.65±0.03	56.7±2.9
Model 5	77.90±0.13	124.90±0.06	1.77±0.01	110.2±0.5	12.83±0.07	59.5±1.6
Model 6	77.59±0.07	125.67±0.09	1.79±0.02	109.6±0.2	12.82±0.05	58.3±2.4

*Pressure at distal ends of terminal segments in fully developed trees.
†Mean diameter of terminal segments (approx. normally distributed for each model, SD approx. 30 μm).
‡Maximum number of bifurcation levels.

where r_L and r_S denote the radii of the larger and smaller daughter segments of segment *i*. Vessels serving transport of blood across larger distances have been classified as distributing (or conveying) vessels.[54] They show highly asymmetric bifurcations (i.e., $\xi_{rad} \ll 1$) and predominantly give off small side branches, which carry only little flow in comparison with the mainstream flow of the parent vessel. On the other hand, vessels with predominantly symmetric bifurcations (i.e., ξ_{rad} close to 1), quickly branch into numerous subtrees of similar structure, thereby splitting blood flow evenly into small portions ready for being delivered into the surrounding tissue (delivering type of vessels[54]).

Figure 6 shows the estimated PDF of the local symmetry index ξ_{rad} for models 4, 5, and 6. To assess the stability of the results, ten realizations for each model were generated by means of different sequences of pseudorandom numbers for tossing new terminal locations. The resulting distributions of ξ_{rad} were significantly different for all realizations of different models (Kolmogorov–Smirnov test, $p < 0.001$). We observe that staged growth reduces the portion of highly symmetric bifurcations (i.e., ξ_{rad} close to 1) in favor of an increasing number of asymmetric bifurcations (i.e., $\xi_{rad} \ll 1$) and the mean value of the distribution slightly shifts to the left from $\xi_{rad} = 0.60 \pm 0.22$ in model 4 to $\xi_{rad} = 0.56 \pm 0.24$ in model 5 and to $\xi_{rad} = 0.57 \pm 0.23$ in model 6.

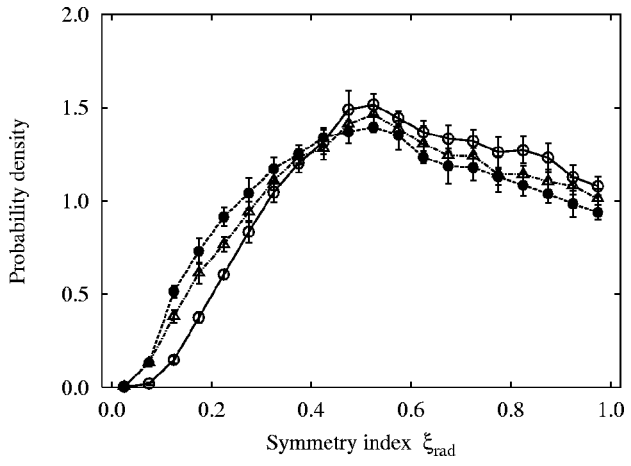

FIGURE 6. Estimated probability density (mean ±SD) of symmetry index ξ_{rad}, Eq. (35), for ten realizations of model 4 (solid line with open circles), model 5 (dashed line with solid circles), and model 6 (dashed-dotted line with open triangles).

Since bifurcation symmetry and bifurcation levels are two related descriptors of binary arterial trees (the existence of a large number of bifurcation levels generally reflects a lower degree of bifurcation symmetry[35]), we applied an ordering scheme for segments based on their bifurcation level Λ_{bif}.[53] The bifurcation level (or generation number) $\Lambda_{bif}(i)$ of a particular segment *i* within a tree is defined as the number of proximal bifurcations along the path from the respective segment towards the root segment i_{root} [i.e., $\Lambda_{bif}(i_{root}) = 0$ and the highest bifurcation level is reached by one or several terminal segments]. For the cases studied, Table 3 suggests that staged growth tends to raise the maximum bifurcation level of CCO trees. Although this effect in the bifurcation levels is small (yielding $F = 3.49$ with $p < 0.05$ for the overall *F* test of analysis of variance), it is (i) stable and (ii) consistent with the behavior of the local symmetry index. In summary, staged growth in models 5 and 6 induces a more asymmetric character in the overall structure of the model trees, indicating an increased portion of ''conveying'' types of vessels. This behavior is consistent with the visual appearance of models 5 and 6 regarding large conveying vessels, which comprise the main vessels at the epicardial surface (top) and the transmural arteries branching out at right angles into the myocardial wall.

The broad distribution of ξ_{rad} in Fig. 6 illustrates that symmetry is highly variable, i.e., both symmetric and very asymmetric bifurcations can be observed within each model. This result is in good agreement with data reported by VanBavel and Spaan[43] for the porcine coronary arterial tree regarding the overall shape of the distribution as well as the mean value given by these authors (0.511 ± 0.243); only the portion of very symmetric

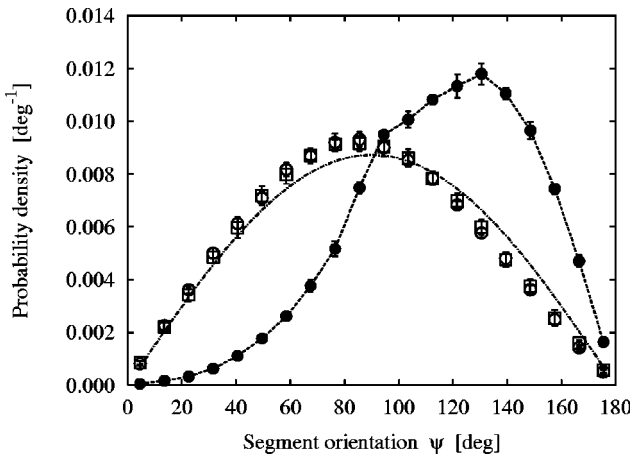

FIGURE 7. Segment orientation for ten realizations of model 6. Estimated probability density (mean ± SD) of the angle ψ between segment orientation and coordinate axes, relative to the *x* axis (open circles), the *y* axis (open squares), and the *z*-axis (dashed line, solid circles). The dashed-dotted line indicates the theoretical probability density function for randomly oriented segments, Eq. (36).

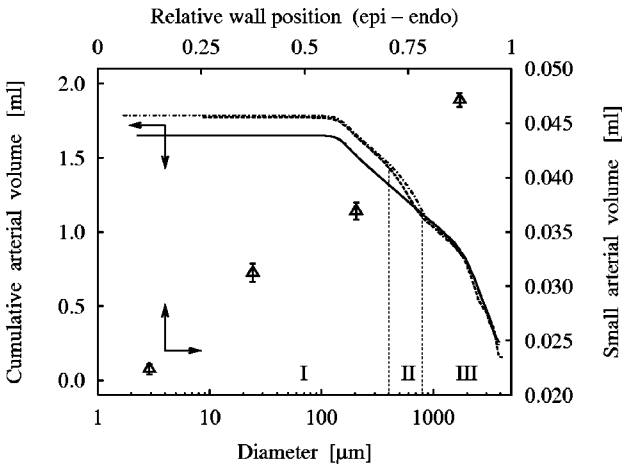

FIGURE 8. Cumulative distribution of intravascular volume (mean values for ten realizations of each model) as a function of segment diameter (starting from the largest diameters, lower *x* axis, left *y* axis) for model 4 (solid line), model 5 (dashed line), and model 6 (dashed-dotted line). Vertical lines separate regions of different classes of segments (see the text). Symbols represent small arterial volume (diameter < 200 μm) in four layers of the epicardial wall for ten realizations of model 6 (mean ± SD, upper *x* axis, right *y* axis).

bifurcations is overestimated by the model trees. Moreover, our model predictions of symmetry are consistent with the experimental findings of Zamir and Chee[52] for human coronary arteries.

Anisotropic Effects of Staged Growth

Staged growth—due to the special form of the stochastic process applied during the generation of new terminal locations [cf. Eqs. (28)–(30)]—defines a reference direction in space. Therefore, one would expect certain properties of our model trees to exhibit more or less pronounced anisotropic effects. As a most direct indicator of anisotropy, we evaluated the distribution of segment orientations with respect to the underlying Cartesian coordinate system. Figure 7 shows the distribution of the angle ψ between segment orientation and the *x*, *y*, and *z* axes, averaged for ten realizations of model 6 (the behavior of model 5 is quite similar and not shown in Fig. 7). As can be seen, the distributions relative to the *x* and *y* axes are nearly identical, almost symmetric about $\psi = 90°$, and closely follow the theoretical curve for the distribution $p(\psi)$ of randomly oriented segments relative to an arbitrary reference direction,

$$p(\psi) = \tfrac{1}{2} \sin \psi. \tag{36}$$

Small deviations from the theoretical (isotropic) shape are clearly attributable to the tree structure and the deterministic process of optimization. However, the distribution relative to the *z* axis, i.e., the (negative) direction of staged growth, is markedly biased towards $\psi = 180°$: the frequency of angles $\psi < 90°$ decreases and the distribution is now dominated by angles $\psi > 90°$, i.e., the distribution of ψ gets significantly right skewed (skewness -0.42) with its mean shifted from $\psi = 86°$ to $\psi = 116°$. In models 5 and 6 segments with $\psi \approx 90°$ represent the large arteries running at the epicardial surface. In contrast, in model 4 segments with $\psi \approx 90°$ are randomly arranged within the perfusion volume, and segment directions are isotropically distributed relative to each coordinate axis.

The observed anisotropy in segment orientation relative to the *z* axis proves to be an immediate consequence of staged growth and the direction in which the zones of vascular growth propagate. Interestingly, the distribution of bee-line angles φ (defined as the angle between the direction of blood transport through a segment and the straight line joining the distal end of that segment with the inlet of the tree) remains practically unaffected. Since φ is a measure for the deviation in the local direction of blood flow from the direction of direct transport from the inlet of the tree to the distal end point of the respective segment, staged growth conserves this specific property of blood transport.

Intravascular Volume

Changing the growth process from conventional to staged raises the final total intravascular volume of the model trees generated (cf. Table 3). In models 5 and 6 staged growth is aimed at arranging large segments preferably near the epicardial surface, and the subset of major conveying vessels in such a way as to dive into the

myocardium as transmural arteries. Hence, one might expect that the major contribution to the observed increase in intravascular volume is due to this latter class of segments. Figure 8 compares models 4, 5, and 6 with respect to the cumulative distribution of intravascular volume V_{iv} as a function of segment diameter. The increase in V_{iv} by 7.3% (8.5%) from model 4 to model 5 (model 6) mainly originates from segments with diameters in the range from 400 to 800 μm (class II). In particular, Fig. 8 shows that the total volume of the large arteries with diameters down to 200 μm is about 1.6 ml/100 g tissue for models 5 and 6 (assuming a specific mass of 1 g/ml for heart tissue[40]); this value is in excellent agreement with experimental data for the coronary arterial tree as reviewed by Spaan.[39] The volume for the small arteries $<$ 200 μm in diameter amounts to about 0.2 ml/100 g tissue; clearly, this value is much too small compared with respective data from the literature.[39,47] However, the model trees were arbitrarily terminated at 6000 terminal segments, whereas VanBavel and Spaan[43] have estimated the total number of end segments (diameters between 5 and 10 μm) to be about 5.5×10^6/100 g tissue, i.e., three orders of magnitude higher than in our model trees; therefore, the above value for the small arteries is not inconsistent with experimental findings. In addition, we have also evaluated the distribution of small arterial volume over the myocardial wall: the volume ratio between subendocardial and subepicardial layers was 1.0 for model 4, 1.3 for model 5, and 2.1 for model 6. For model 6, this ratio as well as the approximately linear increase in small arterial volume from epi- to endocardial layers (Fig. 8) is in excellent agreement with experimental data reported by Wüsten *et al.*[47] (Note that this volume ratio is conserved when the number of terminals is increased to more realistic values.) This indicates that model 6 provides the most consistent description of this aspect of the myocardial vasculature among the models considered.

To visually trace segment classes within our model trees, we chose a different color representation for segments belonging to class II (green) as well as for segments with smaller and larger diameters (red for class I and blue for class III, respectively), cf. Fig. 5(b). As Fig. 5(b) demonstrates, the additional amount of total intravascular volume generated by staged growth is attributable to segments which build up the bunch of conveying-type vessels (green) that dive into the myocardium as transmural arteries almost at right angles from the large vessels at the epicardial surface (blue). These findings confirm that the increase of the total intravascular volume of models 5 and 6 is mainly caused by those segments which also comprise the structural changes induced by staged growth.

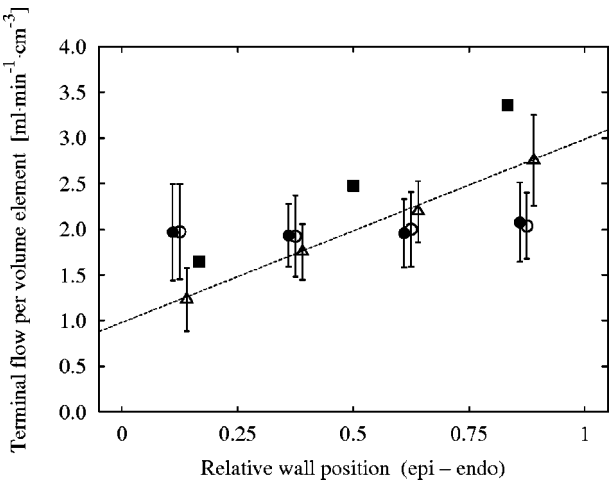

FIGURE 9. Transmural distribution of terminal flows. *y* axis: mean and standard deviation SD of terminal flows per volume element (0.4 cm^3) in four successive layers of the perfusion volume parallel to the epicardial surface for one realization of model 4 (open circles), model 5 (solid circles), and model 6 (open triangles); the displayed mean values are stable within each model class (for ten realizations their SD was 2.3% for model 4, 2.1% for model 5, and 1.5% for model 6). Solid squares indicate experimental flow data of Austin *et al.*, (Ref. 2) normalized with respect to the current volume element size. *x* axis: relative wall position from epi- to endocardial surface (tick marks represent the bounds of the four layers). The dashed line indicates the regression line through the data points of model 6 (slope 2.0, intercept 0.98).

Transmural Distribution of Terminal Flows

Figure 9 compares models 4, 5, and 6 with respect to the mean spatial density of terminal flows in four successive layers of the perfusion volume parallel to the xy plane (i.e., parallel to the epicardial surface). Each layer was cut into 63 square slabs of 1 cm$\times$1 cm$\times$0.4 cm in dimension, and the overall terminal flow per volume element of 0.4 cm^3 was recorded and averaged to yield the values for the mean and standard deviation (SD) for each layer as displayed in Fig. 9. For models 4 and 5 there is no significant difference in the density of terminal flows, neither between the layers, nor between the models, suggesting that the flow distribution is approximately uniform (χ^2 test, $p>0.05$). Since all model trees were generated under the boundary condition of equal terminal flows, the distribution of flows directly reflects the spatial distribution of terminal locations. Therefore, this result confirms that the actual distribution of terminals complies with the prescribed uniform distribution, i.e., staged growth succeeds to generate the desired distribution, and the existing tree structure does not significantly disturb it. In particular, the same arguments hold for model 6, where the prescribed distribution of terminals along the z direction is linear, Eq. (24). Moreover, the data points for model 6 show that the endocardial flow is approximately twice that of the epicardial flow.

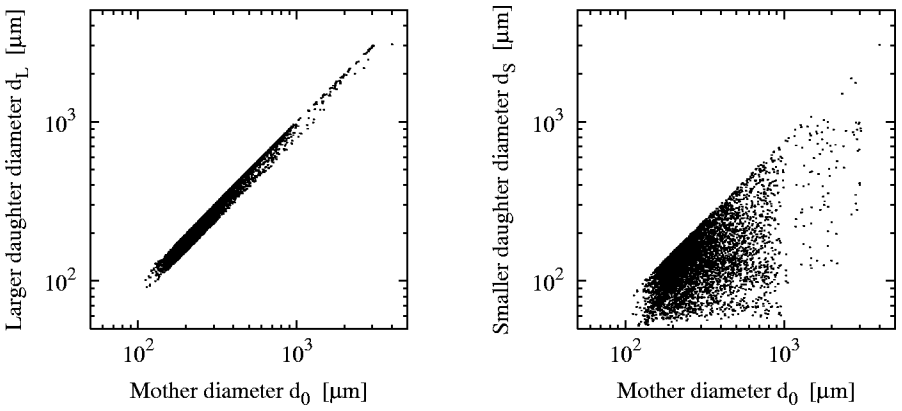

FIGURE 10. Diameters of parent and daughter segments for each bifurcation in one realization of model 6. Left: diameter d_L of larger (i.e., thicker) daughter as a function of the diameter d_0 of the parent segment (squared correlation coefficient $R^2=0.99$, $p<0.001$). Right: diameter d_S of smaller (i.e., thinner) daughter as a function of the diameter d_0 of the parent segment ($R^2=0.47$, $p<0.001$).

This ratio is in excellent agreement with experimental data reported by Austin *et al.*[2] for arrested, maximally vasodilated hearts in dogs; only the absolute flow values are systematically underestimated by model 6.

Figure 9 also provides a convenient estimate for the relative dispersion RD = SD/mean of terminal flows. For volume elements of size 0.4 cm^3 we obtain a mean relative dispersion of terminal flows of about 20% for model 4, 18% for model 5, and 19% for model 6; these values are in good agreement with experimental results reported by Bassingthwaighte *et al.*[3] However, it should be noted that our RD values do not reflect spatial flow heterogeneity as caused by the branching pattern of the trees (since terminal flows are assumed equal), but rather indicate the ''residual flow heterogeneity''[32] due to the random arrangement of terminal locations within the perfusion volume (cf. King *et al.*[19]) and the tree already in existence.

Segment Diameters and Tree Topology

We first consider the relation between diameters of parent and daughter segments: the symbols in Fig. 10 represent the diameter of the larger and smaller daughter (d_L and d_S), respectively, over the whole range of diameters of bifurcating (mother) segments (d_0). In good agreement with data from the literature[43] reported for the porcine coronary arterial tree with diameters ranging approximately from 10 to 2000 μm, we observed (i) d_L to be always of the same order of magnitude as d_0, whereas d_S may be considerably smaller than d_0 up to one order of magnitude; and (ii) we found the variation of d_S over d_0 to be five to ten times larger than that of d_L. It should be mentioned that the experimental data set contained bifurcations with $d_L > d_0$ which cannot be represented by the model trees, cf. Eq. (1).

Next, we focus on topological properties of the model trees and compare our computational results with detailed anatomical data of the pig coronary arterial tree, presented by Kassab *et al.*[16] These authors have introduced a ''diameter-defined Strahler system'' to classify the treelike structure of the coronary arteries according to tree topology and segment diameter. Figure 11 shows the number of elements (i.e., classes of segments having the same diameter-defined Strahler order) in consecutive classes, plotted against the mean element diameter within a respective class. Apart from the lower end of element classes, the rate at which the number of elements increases with decreasing mean element diameter is in good agreement with the experimental data set. However, both experimental data and model trees cover the same range of 11 order numbers, although their smallest element diameters differ by about an order of magnitude. This is probably due to an artifact of CCO trees, caused by the arbitrary cutoff in the tree structure at the prescribed number of terminal segments, leaving too large a number of terminal subtrees in a highly symmetric state.

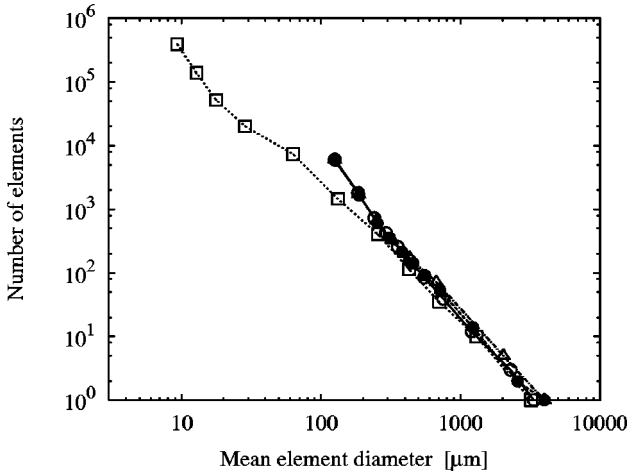

FIGURE 11. Number of elements in classes of diameter-defined Strahler orders, represented by their mean element diameters. Corrected total number of elements in each order of the pig RCA tree (Ref. 16) (open squares), calculated number of elements in model 4 (open circles), model 5 (solid circles), and model 6 (open triangles).

DISCUSSION

The major concern of the present study was to model inhomogeneous vascular structures by the method of CCO. In particular, we focused on the variations between epi- and endocardial branching patterns in the coronary arterial tree. Casting the original process of tree generation into a nonstationary form by means of an additional time-dependent boundary condition yields successive zones of vascular growth (''staged growth''). We consider staged growth a mechanistic approach not aimed at modeling the details of actual vascular growth.[11] Nevertheless, the model reproduces some important structural and functional parameters of the coronary arterial tree in good agreement with experimental data. In the following discussion we consider the various idealizing assumptions and the resulting limitations of the model.

The basic model assumptions of CCO include that blood flow conditions are laminar and steady state and the hydrodynamic resistance R of each segment obeys Poiseuille's law,[7]

$$R=\left(\frac{8\eta}{\pi}\right)\frac{l}{r^4}, \tag{37}$$

where l and r are length and internal radius of the respective segment and η is the viscosity of blood. This is an idealization, and blood flow actually depends on the dimensionless Reynolds and Womersley numbers;[7] only if both of these numbers are much smaller than 1, deviations from the above conditions can be neglected. Kassab *et al.*[18] have pointed out, that for the coronary arteries the Womersley numbers are smaller than 1 and coronary blood flow may in a first approximation be treated as quasisteady. In the largest coronary arteries, however, Reynolds numbers are of the order of 100; thus, Poiseuille's formula must be corrected here. Additionally, CCO omits flow resistance due to branching and due to entrance effects caused by the finite length of arterial segments. Since all these effects raise the hydrodynamic resistance, application of Poiseuille's law in CCO models generally underestimates the actual resistance to blood flow.

Another idealization of CCO refers to blood, which is treated as an ideal Newtonian viscous fluid with constant viscosity η. However, it is well known that blood viscosity depends on the shear rate between blood and vessel walls, on the vessel diameter, on the hematocrit, and on temperature.[8] Since blood viscosity also determines flow resistance, η is an important parameter in CCO models. As could be shown in a previous study[37] on the basis of experimental data,[21,22] the variation of shear rates in CCO models gives rise to an average variation of viscosity of about 5%. We therefore think that it is a good approximation for CCO trees to neglect the dependency of η on shear rate. For the range of vessel diameters observed in CCO trees, in particular for diameters less than about 500 μm, viscosity depends on vessel diameter: *in vivo* measurements reported by Pries *et al.*[29] suggest that effective blood viscosity decreases with decreasing vessel diameter in accordance with the Fahraeus–Lindqvist effect down to diameters of about 30 μm; for vessel diameters below 30 μm, effective viscosity showed a marked increase *in vivo*, in contrast to *in vitro* measurements in blood-perfused glass tubes. It is highly desirable to include these *in vivo* rheological data into future developments of the CCO model to obtain more realistic values for flow resistance and pressure drops in CCO trees.

In CCO trees, the relation between mother and daughter diameters at each bifurcation is obtained from a power law as given in Eq. (1). The exponent γ is related to the change of total cross-sectional area along bifurcations and is a major determinant of the pressure profile.[32] In the present study we have used a constant value of $\gamma=2.55$ throughout the tree;[1] as could be shown earlier,[32] this choice of γ renders the pressure profile of CCO trees in reasonable agreement with experimental data, whereas $\gamma>2.55$ yields too high a pressure drop in the larger branches of the tree. Although $\gamma=2.55$ is not inconsistent with other measured data,[23,41,51,52] recent experimental data for the coronary arterial tree[17,43] as well as theoretical considerations[45] suggest γ to vary with vessel diameter from γ close to 3 at the arteriolar level up to γ close to 2 for large arteries. We think that using different values of γ for segments of different caliber might improve branching patterns and pressure profiles of CCO model trees.

Central to the method of CCO is the application of an optimality principle, which determines not only the geometry of single bifurcations (such as branching angles and length ratios of parent and daughter segments) but also controls the global topological structure of CCO trees. The process of optimization is influenced by the choice of boundary conditions, in particular by the assumption of equal terminal pressures and flows: In a binary branching tree of given topology and segment locations the boundary conditions used in the present model yield a unique solution for all segment diameters.[32] Maintaining the boundary conditions determines how diameters change during geometric optimization. The resulting bifurcations therefore reflect the combination of optimization for minimum volume and a distribution of resistance throughout the tree needed to fulfill the boundary conditions of constant terminal pressures and flows. Different approaches related to the principle of functional optimality of arterial bifurcations have been reported in the literature. As Griffith and Edwards[9] have pointed out, these approaches may be classified as

either flow independent, such as minimum vascular surface area[48] and minimum intravascular volume[14], or as flow dependent, such as minimum wall shear stress[49] and minimum power loss,[48] or as a combination of both.[24,25,42] (For an extensive review of these models see Zamir,[48] Woldenberg and Horsfield,[46] and Griffith and Edwards.[9] Note that for the special choice of $\gamma = 3$, volume and power are optimized simultaneously.[46]) Flow-independent optimality principles have been previously discussed for CCO trees, and minimizing intravscular volume has proved to be a ''golden standard'' both with respect to morphometric properties and shear-stress variability.[34,37] Although minimum intravascular volume seems a physiologically reasonable choice (since blood is costly to construct and to maintain[20,24,38] and because the arterial side of the circulation represents a low-volume/high-pressure system[9]), it is probably not the only principle at work[48] and it might not be adequate for all parts of the cardiovascular system, having different functions and modes of operation.[50] [In this context it is interesting to note that the method of staged growth combines the principle of minimum volume with an additional (time-dependent) boundary condition regarding the actual zone of vascular growth to generate the desired epi-/endocardial structures; as a consequence of generating these additional structures, the total intravascular volume increases.] Hence, the evaluation of flow-dependent or even combined optimization principles within the framework of CCO remains an interesting question for coming studies. However, it should be kept in mind that for complex biological systems any optimality principle is only a hypothesis,[17] and within this context we understand the method of CCO as a contribution to validate such principles by detailed modeling and comparison with experimental findings.

Although the CCO model generates static branching patterns, assuming arrested hearts and maximal vasodilation, their structure cannot be discussed without considering the beating of the heart, in particular with respect to the interaction of heart contraction and coronary resistance. The ingredients to the method of staged growth, formulated as an additional (time-dependent) boundary condition in the original algorithm of CCO, are derived from the morphology of real coronary arterial trees, i.e., from the spatial arrangement of large epicardial and transmural arteries and from the distribution of small intramural arteries and arterioles over the myocardial wall. In the normal beating heart—despite an increased extra-vascular resistance in endocardial layers—the transmural flow distribution is approximately homogeneous, suggesting a decreased subendocardial resistance due to a better vascularization as a possible mechanism to compensate for the compression during heart contraction.[10,47] This hypothesis was confirmed by experiments on resting and maximally vasodilated hearts, where both flow and small arterial volume were found to be higher in the subendocardium than in the subepicardium.[2,47] Only model 6, where the distribution of terminal segments is assumed to (linearly) increase from epi- to endocardial layers, provides an acceptable description of both transmural flow and small arterial volume distribution.

Apart from intravascular volume, a second important physiological parameter the structure of an arterial tree model should correctly predict, is the pressure as a function of segment diameter. At the 250-μm-diam level, mean pressure has dropped from 100 mm Hg perfusion pressure down to about 80 mm Hg; this value is in good agreement with data reported by Chilian *et al.*[4] for intense coronary vasodilation. As can be seen from Table 3, pressure in terminal segments (with mean diameters of about 120 μm) is approximately 78 mm Hg for models 4, 5, and 6. This result indicates that the predicted pressure drop is too small for diameters <250 μm compared with the data from Chilian *et al.* (Yet, models 5 and 6 predict subepicardial pressures higher than subendocardial pressures, e.g., 88 mm Hg vs 83 mm Hg for 300 μm segments; this trend is consistent with the transmural differences reported by Chilian.[5]) The pressure profile is mainly determined by the variation of segmental resistance [i.e., segment diameter and length, cf. Eq. (37)] and the number of segments along the branching pattern of the tree. Since segment diameters enter resistance with their fourth power, much of the observed discrepancies in pressure may be attributed to the variation of segment diameters along bifurcations. This variation is characterized by Eq. (1), and as we have noted above, a constant exponent γ for the whole tree is probably too strong an idealization. These arguments are supported by the view that in the coronary arterial tree there is no continuous branching pattern that extends from large down to very small arteries.[40]

In conclusion, this study presents an extension to the method of CCO, which allows us to model spatial variations in the structure of arterial trees by means of an additional time-dependent boundary condition. In particular, we have explored a three-dimensional model of the coronary arterial tree with the aim to describe the different branching patterns of the subendocardium and subepicardium. Although the model contains quite a number of considerable simplifications, its predictions regarding the diameter ratios of parent and daughter segments, the distribution of symmetry, the transmural distribution of flow, the volume of large arteries as well as the ratio of small arterial volume in subendocardial and subepicardial layers are in good agreement with experimental data. The present study suggests that the hypothesis of minimum intravascular volume alone is not sufficient to explain the structural variations observed in the coronary arterial tree. Further work is required to im-

prove the model, in particular regarding its idealizing assumptions on the validity of Poiseuille's law, on blood rheology, and on the bifurcation exponent.

ACKNOWLEDGMENTS

The authors gratefully acknowledge the critical comments and valuable suggestions of the unknown reviewers of this study.

REFERENCES

[1] Arts, T., R. T. I. Kruger, W. VanGerven, J. A. C. Lambregts, and R. S. Reneman. Propagation velocity and reflection of pressure waves in the canine coronary artery. *Am. J. Physiol.* 237:H469–H474, 1979.

[2] Austin, Jr., R. E., N. G. Smedira, T. M. Squiers, and J. I. E. Hoffman. Influence of cardiac contraction and coronary vasomotor tone on regional myocardial blood flow. *Am. J. Physiol.* 266:H2542–H2553, 1994.

[3] Bassingthwaighte, J. B., R. B. King, and S. A. Roger. Fractal nature of regional myocardial blood flow heterogeneity. *Circ. Res.* 65:578–590, 1989.

[4] Chilian, W. M., S. M. Layne, E. C. Klausner, C. L. Eastham, and M. L. Marcus. Redistribution of coronary microvascular resistance produced by dipyridamole. *Am. J. Physiol.* 256:H383–H390, 1989.

[5] Chilian, W. M. Microvascular pressures and resistances in the left ventricular subepicardium and subendocardium. *Circ. Res.* 69:561–570, 1991.

[6] Fulton, W. F. M. Morphology of the myocardial microcirculation. In: Microcirculation of the Heart, edited by H. Tillmanns, W. Kübler, and H. Zebe. Berlin: Springer, 1982, pp. 15–25.

[7] Fung, Y. C. Biomechanics: Motion, Flow, Stress, and Growth. New York: Springer, 1990, pp. 155–195.

[8] Fung, Y. C. Biomechanics: Mechanical Properties of Living Tissues. New York: Springer, 1993, pp. 66–108.

[9] Griffith, T. M. and D. H. Edwards. Basal EDRF activity helps to keep the geometrical configuration of arterial bifurcations close to the Murray optimum. *J. Theor. Biol.* 146:545–573, 1990.

[10] Hoffman, J. I. E. and J. A. E. Spaan. Pressure-flow relations in coronary circulation. *Physiol. Rev.* 70:331–390, 1990.

[11] Hudlicka, O., M. Brown, and S. Egginton. Angiogenesis in skeletal and cardiac muscle. *Physiol. Rev.* 72:369–417, 1992.

[12] James, T. N. Anatomy and pathology of small coronary arteries. In: Coronary Circulation: From Basic Mechanisms to Clinical Implications, edited by J. A. E. Spaan, A. V. G. Bruschke, and A. C. Gittenberger-DeGroot. Dordrecht: Martinus Nijhoff, 1987, pp. 13–23.

[13] Kalos, M. H., and P. A. Whitlock. Monte Carlo Methods. New York: Wiley, 1986, Vol. 1, pp. 40–48.

[14] Kamiya, A. and T. Togawa. Optimal branching structure of the vascular tree. *Bull. Math. Biophys.* 34:431–438, 1972.

[15] Karch, R., F. Neumann, M. Neumann, and W. Schreiner. A three-dimensional model for arterial tree representation, generated by constrained constructive optimization. *Comput. Biol. Med.* 29:19–38, 1999.

[16] Kassab, G. S., C. A. Rider, N. J. Tang, and Y.-C. B. Fung. Morphometry of pig coronary arterial trees. *Am. J. Physiol.* 265:H350–H365, 1993.

[17] Kassab, G. S. and Y. C. B. Fung. The pattern of coronary arteriolar bifurcations and the uniform shear hypothesis. *Ann. Biomed. Eng.* 23:13–20, 1995.

[18] Kassab, G. S., J. Berkley, and Y. C. B. Fung. Analysis of pig's coronary arterial blood flow with detailed anatomical data. *Ann. Biomed. Eng.* 25:204–217, 1997.

[19] King, R. B., L. J. Weissman, and J. B. Bassingthwaighte. Fractal descriptions for spatial statistics. *Ann. Biomed. Eng.* 18:111–121, 1990.

[20] LaBarbera, M. Principles of design of fluid transport systems in zoology. *Science* 249:992–999, 1990.

[21] Lipowsky, H. H. and B. W. Zweifach. Methods for the simultaneous measurement of pressure differentials and flows in single unbranched vessels of the microcirculation for rheological studies. *Microvasc. Res.* 14:345–361, 1977.

[22] Lipowsky, H. H., S. Usami, and S. Chien. *In vivo* measurements of the apparent viscosity and microvessel hematocrit in the mesentery of the cat. *Microvasc. Res.* 19:297–319, 1980.

[23] Mayrovitz, H. N. and J. Roy. Microvascular blood flow: Evidence indicating a cubic dependence on arteriolar diameter. *Am. J. Physiol.* 245:H1031–H1038, 1983.

[24] Murray, C. D. The physiological principle of minimum work. I. The vascular system and the cost of blood volume. *Proc. Natl. Acad. Sci. USA* 12:207–214, 1926.

[25] Murray, C. D. The physiological principle of minimum work applied to the angle of branching of arteries. *J. Gen. Physiol.* 9:835–841, 1926.

[26] Neumann, F., M. Neumann, R. Karch, and W. Schreiner. Visualization of computer-generated arterial model trees. In: Simulation Modelling in Bioengineering, edited by M. Cerrolaza, D. Jugo, and C. A. Brebbia. Southampton, U.K.: Computational Mechanics, 1996, pp. 259–268.

[27] Neumann, F., W. Schreiner, and M. Neumann. Computer simulation of coronary arterial trees. *Adv. Eng. Software* 28:353–357, 1997.

[28] Papoulis, A. Probability, Random Variables, and Stochastic Processes. New York: McGraw-Hill, 1981, pp. 279–332.

[29] Pries, A. R., T. W. Secomb, T. Geßner, M. B. Sperandio, J. F. Gross, and P. Gaehtgens. Resistance to blood flow in microvessels *in vivo*. *Circ. Res.* 75:904–915, 1994.

[30] Rosen, R. Optimality Principles in Biology. London: Butterworth, 1967, pp. 40–60.

[31] Schreiner, W. Computer generation of complex arterial tree models. *J. Biomed. Eng.* 15:148–149, 1993.

[32] Schreiner, W., and P. Buxbaum. Computer-optimization of vascular trees. *IEEE Trans. Biomed. Eng.* 40:482–491, 1993.

[33] Schreiner, W., M. Neumann, F. Neumann, S. M. Roedler, A. End, P. Buxbaum, M. R. Müller, and P. Spieckermann. The branching angles in computer-generated optimized models of arterial trees. *J. Gen. Physiol.* 103:975–989, 1994.

[34] Schreiner, W., F. Neumann, M. Neumann, A. End, S. M. Roedler, and S. Aharinejad. The influence of optimization target selection on the structure of arterial tree models generated by constrained constructive optimization. *J. Gen. Physiol.* 106:583–599, 1995.

[35] Schreiner, W., F. Neumann, M. Neumann, A. End, and M. R. Müller. Structural quantification and bifurcation symmetry in arterial tree models generated by constrained constructive optimization. *J. Theor. Biol.* 180:161–174, 1996.

[36] Schreiner, W., F. Neumann, M. Neumann, A. End, and S. M. Roedler. Anatomical variability and functional ability of vascular trees modeled by constrained constructive optimization. *J. Theor. Biol.* 187:147–158, 1997.

[37] Schreiner, W., F. Neumann, R. Karch, M. Neumann, S. M. Roedler, and A. End. Shear stress distribution in arterial tree

models, generated by constrained constructive optimization. *J. Theor. Biol.* 198:27–45, 1999.
[38] Sherman, T. F. On connecting large vessels to small: The meaning of Murray's law. *J. Gen. Physiol.* 78:431–453, 1981.
[39] Spaan, J. A. E. Coronary diastolic pressure-flow relation and zero flow pressure explained on the basis of intramyocardial compliance. *Circ. Res.* 56:293–309, 1985.
[40] Spaan, J. A. E. Coronary Blood Flow: Mechanics, Distribution, and Control. Dordrecht: Kluwer Academic, 1991, pp. 37–67.
[41] Suwa, N., T. Niwa, H. Fukasawa, and Y. Sasaki. Estimation of intravascular blood pressure gradient by mathematical analysis of arterial casts. *Tohoku J. Exp. Med.* 79:168–198, 1963.
[42] Uylings, H. B. M. Optimization of diameters and bifurcation angles in lung and vascular tree structures. *Bull. Math. Biol.* 39:509–520, 1977.
[43] VanBavel, E. and J. A. E. Spaan. Branching patterns in the porcine coronary arterial tree: Estimation of flow heterogeneity. *Circ. Res.* 71:1200–1212, 1992.
[44] Van Beek, J. H. G. M., S. A. Roger, and J. B. Bassingthwaighte. Regional myocardial flow heterogeneity explained with fractal networks. *Am. J. Physiol.* 257:H1670–H1680, 1989.
[45] West, G. B., J. H. Brown, and B. J. Enquist. A general model for the origin of allometric scaling laws in biology. *Science* 276:122–126, 1997.
[46] Woldenberg, M. J. and K. Horsfield. Relation of branching angles to optimality for four cost principles. *J. Theor. Biol.* 122:187–204, 1986.
[47] Wüsten, B., D. D. Buss, H. Deist, and W. Schaper. Dilatory capacity of the coronary circulation and its correlation to the arterial vasculature in the canine left ventricle. *Basic Res. Cardiol.* 72:636–650, 1977.
[48] Zamir, M. Optimality principles in arterial branching. *J. Theor. Biol.* 62:227–251, 1976.
[49] Zamir, M. The role of shear forces in arterial branching. *J. Gen. Physiol.* 67:213–222, 1976.
[50] Zamir, M. Shear forces and blood vessel radii in the cardiovascular system. *J. Gen. Physiol.* 69:449–461, 1977.
[51] Zamir, M., J. A. Medeiros, and T. K. Cunningham. Arterial bifurcations in the human retina. *J. Gen. Physiol.* 74:537–548, 1979.
[52] Zamir, M. and H. Chee. Branching characteristics of human coronary arteries. *Can. J. Physiol. Pharmacol.* 64:661–668, 1986.
[53] Zamir, M. and H. Chee. Segment analysis of human coronary arteries. *Blood Vessels* 24:76–84, 1987.
[54] Zamir, M. Distributing and delivering vessels of the human heart. *J. Gen. Physiol.* 91:725–735, 1988.
[55] Zamir, M. Flow strategy and functional design of the coronary network. In: Coronary Circulation: Basic Mechanisms and Clinical Relevance, edited by F. Kajiya, G. A. Klassen, J. A. E. Spaan, and J. I. E. Hoffman. Tokyo: Springer, 1990, pp. 15–40.